Published in final edited form as:
Methods. 2012 May ; 57(1): 40–46. doi:10.1016/j.ymeth.2012.03.026.

Single-molecule investigation of G-quadruplex using a nanopore sensor

Jiwook Shim[a,b,*] and **Li-Qun Gu**[c,d,*]

[a]Department of Electrical and Computer Engineering, University of Illinois at Urbana-Champaign, Urbana, IL 61801, USA

[b]Micro and Nanotechnology Laboratory, University of Illinois at Urbana-Champaign, Urbana, IL 61801, USA

[c]Department of Biological Engineering, University of Missouri, Columbia, MO 65211, USA

[d]Dalton Cardiovascular Research Center, University of Missouri, Columbia, MO 65211, USA

Abstract

This review article introduces the nanopore single-molecule method for the study of G-quadruplex nucleic acid structures. Single G-quadruplexes can be trapped into a 2 nm protein pore embedded in the lipid bilayer membrane. The trapped G-quadruplex specifically blocks the current through the nanopore, creating a signature event for quantitative analysis of G-quadruplex properties, from cation-determined folding and unfolding kinetics to the interactions with the protein ligand. The nanopore single-molecule method is simple, accurate, and requires no labels. It can be used to evaluate G-quadruplex mechanisms and it may have applications in G-quadruplex-based biosensors, nanomachines, and nanostructure assembly.

Keywords

Nanopore; Alpha-hemolysin; G-quadruplex; Thrombin-binding aptamer; Folding and unfolding; Kinetics

1. Introduction

The bacterial toxin alpha-hemolysin (αHL) is one of protein channels that form molecular-scale pores across the lipid bilayer, called nanopores [1-3]. Structurally, the αHL pore is made up of a 2 nm wide transmembrane β-barrel stem and a mushroom-shaped cap domain that surrounds a nanocavity of 4 nm in width (Fig. 1). The nanocavity is accessible via a 2.6 nm opening (*cis* entrance), and is connected with the β-barrel via a 1.4 nm constriction [4]. When voltage is applied across the membrane, a pico-Ampere ion current passing through the pore can be detected. Due to the nanometer-scale size of the pore, this current can be blocked by target molecules entering the pore. This blockage is very sensitive to the molecular species, to the position of the target molecule, and to the configuration of the pore. This ability gives the nanopore broad applications in diverse single-molecule-based nano-biotechnological applications [5]. The nanopore method has been evaluated in a number of reviews [6-16]. This method has been studied extensively with an eye toward

*Corresponding authors. Addresses: Micro and Nanotechnology Laboratory, University of Illinois at Urbana-Champaign, Urbana, IL 61801, USA. Fax: +1 217 244 6375 (J. Shim), Dalton Cardiovascular Research Center, University of Missouri, Columbia, MO 65211, USA. Fax: +1 573 884 4232 (L.-Q. Gu). shimji@illinois.edu (J. Shim), gul@missouri.edu (L.-Q. Gu).

single-molecule DNA sequencing [6,17-20]. Nanopores have already seen broad use as biosensors for manifold detection of biological substances [21,22] such as polynucleotides [23-29], peptides [30], metal ions [31], second messengers [32], and disease biomarkers [33]. Nanopores can regulate the transportation of various substances across the membrane [34,35]. They can also serve as single-molecule force gauges in the study of molecular interactions [36] and dissociation of a nucleic acid duplexes [37]. Protein nanopores can also be integrated into biochips for real-time biosensing [38,39].

The G-quadruplex is a nucleic acid structure formed by guanine-rich sequences, which are very widespread in the human genome [40-42]. Many in-depth reviews have discussed various G-quadruplex about their structures, metabolisms [43-46] and potentials as drug targets [47-49]. These G-rich nucleic acids can pose a G-quartet when four guanines are tied via hydrogen bond, consequently fold into the G-quadruplex structure by stacking the quartets [43,50-52]. The G-quadruplex has attracted great consideration as therapeutic-target with their relevance to genetic process at telomeres and promoters [53-60]. *In vitro* synthetic G-quadruplexes can be used to construct biosensors [61-64], function as a nanometer-scale machine for various bioprocessing [65,66], and used as building blocks in the design of new nano structures [67]. Recently, we used nanopore single-molecule technology to investigate the entrapment of G-quadruplex in the nanopore [68] and ion-regulated folding/unfolding reactions of the G-quadruplex [69]. This article will discuss the specific methods involved in these findings. Selected topics include the formation of the nanopore, methods of observing single nanopores, data analysis, ways in which nanopores can be used to observe single G-quadruplexes, and an analytical approach to determining the equilibrium G-quadruplex formation constants and the rate constants for the folding and unfolding reactions [69].

Our target is the thrombin-binding aptamer (TBA). This 15 mer G-rich DNA oligonucleotide (GGTTGGTGTGGTTGG) is a widely-used model G-quadruplex. It folds into a compact G-quadruplex with two stacked quartets coordinated by a metal ion [70-73]. The cation species is critical to determining the stability of the G-quadruplex [71]. Upon folding, the TBA G-quadruplex binds with human thrombin to slow down thrombin coagulation [62]. The structure of G-quadruplex has been analyzed via X-ray and nuclear magnetic resonance [43,51,74]. Its folding/unfolding profile has been evaluated using UV spectroscopy, circular dichroism, and differential scanning calorimetry [71,75-78]. The dynamics of the G-quadruplex have been examined using surface plasmon resonance [79], and fluorescence resonance energy transfer [80-85]. Both of these methods require substantial labeling of the target molecules.

2. Methods and results

2.1. Material preparation and embedding of single nanopores in lipid bilayers

In our previous works, all DNA oligonucleotides, including TBA, tagged-TBA, and control species, were synthesized by Integrated DNA Technologies at a PAGE-purification grade, and suspended in TE solution (10 mM Tris and 0.1 mM EDTA at pH 7.2) at 1 mM. The tubes containing DNA solutions were incubated in 90 °C water bath for 15 min, and then slowly restored to room temperature (22 ± 2 °C). Human α-thrombin with a purity of 97.9% was obtained at Haematologic Technologies, Inc. Both DNA and protein were stored at −20 °C in freezer until experiment. Two electrodes were made by placing a Ag/AgCl wire in a salt-bridge containing 0.5% agarose and 3 M KCl. The wild-type αHL protein can be purchased from Sigma–Aldrich Co. LLC., but we synthesized the protein using coupled *in vitro* transcription and translation (IVTT) kit provided by Promega Inc. The characteristics and preparation of the αHL pore are discussed in-depth in previous works and their references [86].

The planar lipid bilayer was formed over a tiny hole in a Teflon film based on the monolayer folding method [87]. The procedure is as follows. The Teflon film was clamped between two custom-made Teflon reservoir chambers (*cis* and *trans*), where it served as a partition. A 100 μm orifice had been punched through the Teflon film. The orifice was coated with a layer of pretreat solvent (hexadecane/pentane at a volume ratio of 1:10). Then the chambers on both sides of the partition were filled with 1 ml of recording solution to the level below the orifice. Ten microliters of lipid solution (1,2-diphytanoyl-*sn*-glycerophosphatidylcholine, Avanti Polar Lipids) was dropped onto the surface of both solutions. The solvent was evaporated within 5 min and a solvent-free lipid monolayer formed at the solution–air interface. Then another 1 ml recording solution was gradually added to each chamber. As the level of solution increased, the lipid monolayers formed along both surfaces of the Teflon partition. When the solutions in both chambers were leveled up above the orifice, the two monolayers met at the orifice and spontaneously formed a lipid bilayer. Two Ag/AgCl electrodes were connected to both solutions to monitor the electrical properties of the lipid bilayer. A qualified bilayer should be highly electrically insulating with a resistance over 100 GΩ and a capacitance of 100–200 pF. The bilayer should also have a low level of electrical noise with the current root-mean-square (I_{RMS}) between 1.2 and 1.8 pA. If the protein pore is not present in the bilayer, there should be no current recorded. When a protein pore is inserted into the lipid bilayer, an ion current through the pore can be immediately recorded at an applied voltage. For example, the ion current of wild-type αHL pore in 1 M KCl (pH 7.2) was 45 pA, recorded at 40 mV.

2.2. Single-nanopore recording setup, measurement, and data processing

When recording the nanopore current, the *cis* chamber was connected to the ground, and the transmembrane voltage was applied through the electrode in *trans* chamber. In this way, the positive voltage generated a *trans*-to-*cis* current flow. The αHL protein was applied to the *cis* chamber from which it is inserted into the lipid bilayer. Nanopores formed in this orientation have a nanocavity domain facing the *cis* solution while the β-barrel entrance to the *trans* solution (Fig. 1a). Both *cis* and *trans* chambers were filled with 1 M monovalent (Na^+, K^+, NH^{4+}, Li^+, or Cs^+) or divalent (Ba^{2+}, Ca^{2+}, or Mg^{2+}) salt solution at pH 7.2. Then 2.5 μM of DNAs was added to the *cis* chamber. Because DNA is negatively charged, the positive voltage pulls DNA into the nanopore. The pico-Ampere ion current was measured using an Axopatch 200A or 200B amplifier (Molecular Devices LLC., Sunnyvale, CA, US) and recorded using an A/D converter of Digidata 1332A or 1440A (Molecular Devices, LLC. Sunnyvale, CA, US). The current traces were recorded at a specific low-pass built-in filtering (e.g. 5 kHz) and sampled at a 3- to 4-fold higher rate (e.g. 20 kHz) using Clampex (Molecular Devices, LLC. Sunnyvale, CA, US). The recorded current traces are then analyzed using Clampfit (Molecular Devices) and Excel (Microsoft Corporation) and SigmaPlot (SPSS). The current amplitude was determined using Gaussian fitting on all point histogram of traces. Every DNA molecule interacting with the nanopore generated a signature with current blockage. The signature characteristics, including the amplitude of the blocked current and the duration of blockage, should be used to identify the target, and to determine the number of signature events, calculate the frequency of occurrence, and quantify the target.

2.3. Discriminating G-quadruplex signatures

To investigate single G-quadruplex molecules, we first need to distinguish the electrical signal produced by the interaction of G-quadruplex with the nanopore. This can be realized by comparing TBA signal with control DNA lacking the ability to form G-quadruplexes, such as $Ctrl_2$ (GATTAGTGTGATTAG). This control oligotide contains 15 nucleotides, like TBA. However, its ability to fold is suppressed because its key guanines have been replaced with adenines. The nanopore current traces for control DNA only show pulse-like, short-

lived block events that reduced ≈90% of the pore conductance and lasted for 349–450 μs in monovalent Li^+, Na^+, K^+, NH_4^+, and Cs^+, and 1280–5700 μs in divalent Ba^{2+}, Mg^{2+}, and Ca^{2+} (Fig. 2). These short events were caused by the translocation of linear-form DNAs through the nanopore. Unlike control DNA, the TBA G-quadruplex produced prolonged blockage events that only partially reduced the pore conductance by 34–50%. These long events can be attributed to the trapping of a single TBA G-quadruplex in the nanocavity of the αHL pore. The duration of long events depends on what cation is used in the recording solution: 0.35 s in Na^+, 4 s in NH_4^+, 12 s in Cs^+, and 17 s in Li^+, K^+, and Ba^{2+} (no long events were observed with Mg^{2+} or Ca^{2+}) (Fig. 2). In addition to long blockages, current traces for TBA also show short-lived blockages with durations of 280–630 μs in monovalent cations and 1490–4100 μs in divalent cations, which is similar to values observed for control DNAs. This can be attributed to the translocation of unfolded TBA through the pore. The observation of both long and short events suggests that TBA in solution presents equilibrium between the folded (G-quadruplex) and unfolded conformations.

TBA G-quadruplex can bind to human α-thrombin with high affinity [62]. This method can be used to confirm that the long duration events are generated by the presence of G-quadruplexes in the nanopore. When the mixture of TBA and thrombin was introduced to the *cis* solution, no long-lived event was observed at any point during the 15 min recording time. This is because most of the TBA was bound to thrombin and there was very little free G-quadruplex in solution to be captured by the pore. Meanwhile the large dimension of TBA·thrombin complex (5.6 × 7.7 × 10 nm [72]) compared with *cis* opening of the pore (2.6 nm) prevents the complex from entering the pore. Because the amount of unfolded TBA decreases as it keeps equilibrium with folded TBA as the latter binds with thrombin, the number of short events for translocation of unfolded TBA also decreases significantly [68].

2.4. Localizing G-quadruplex in the nanopore nanocavity

Signature signals indicate the entrapment of single G-quadruplexes in the nanopore. However, they cannot indicate exactly where within the pore the quadruplex binds. We first evaluated the dimensions of the G-quadruplex and nanopore. The G-quadruplex is 2.1 nm wide, as determined using the diagonal distance between O_3 atoms in a guanine-quartet [73]. This is in similar to that of another G-quadruplex, the 16-base HIV-1 integrase aptamer [88]. When folded, the G-quadruplex is slightly smaller than the 2.6 nm *cis* opening (Fig. 1b) of the pore (nanocavity entrance). For this reason, the G-quadruplex is unlikely to bind at the *cis* opening. Rather, it enters the nanocavity through this opening (Fig. 1c). Because the G-quadruplex is larger than the width of the β-barrel entrance, 1.4 nm (Fig. 1d), the trapped G-quadruplex cannot pass through the β-barrel. We therefore expected that the G-quadruplex would reside in the nanocavity (Fig. 1a) until its molecular configuration changes. Second, the partial blockage of the ion pathway of the pore (≈50% current reduction) is consistent with a scenario in which the G-quadruplex remains in the nanocavity. The volumes of the G-quadruplex (1.5 nm^3) and nanocavity (3.5 nm^3) mean that the large amount of unoccupied space in the nanocavity still permits ion flow. Finally, the current of the long-lived partial blockage is flat, without additional changes. This suggests that when one G-quadruplex is present in the nanocavity, no other molecules can be trapped there to generate interfering signals.

Another valid means of determining the presence of the G-quadruplex within the nanopore is to design engineered TBAs with a signal tags. TBAs have been attached to 6 nts overhang reporters (GACTAC) at the 5′ terminal. The tagged-TBAs retain the ability to form G-quadruplexes, taking on a ball-and-stick (quadruplex and tag) conformation [89]. When trapped in the nanopore, their signatures shows additional level-2 current blockage beyond the long partial blockage (Fig. 3f). The level-2 conductance has been found to be similar to

that of linear DNA translocation. This can be attributed to the tag that enters the β-barrel. Using this method, we verified that TBA is located around the bottom of the nanocavity.

2.5. Auto-unfolding of G-quadruplex with in the nanocavity

The G-quadruplex trapped in the nanocavity can undergo three configuration changes, lengthy staying in the pore, returning to the *cis* solution, or unfolding and leaving the pore through the β-barrel. We observed the long duration events (Fig. 3a), and further observed that ≈80% of long partial blocks are terminated with an ending spike that lasts ≈270 μs and almost fully reduces the pore conductance (Fig. 3b). The characteristics of the terminal-spike, including duration and current amplitude, resemble the short-lived events produced by unfolded DNA translocation (Fig. 3c). Based on this point, we have concluded that the G-quadruplex unfolds in the nanocavity, and the ending-spike that we observed is due to the immediate translocation of unfolded TBA through the β-barrel. This conclusion can be verified experimentally: The duration of ending spikes shortens as voltage increases, which supports the idea that the translocation of linear-form DNA accelerates at high voltages. We have also observed that ≈20% of long events lack ending-spikes (Fig. 3d), which is attributable to return of the G-quadruplex to the *cis* solution without unfolding. The lifetime of the long event for the G-quadruplex does not vary with the voltage (between 90 and 180 mV) [68]. The observation of constant G-quadruplex lifetime at various voltages indicates that the unfolding of the G-quadruplex is a spontaneous rather than a voltage-driven procedure.

2.6. Tracking folding/unfolding kinetics

It has been concluded based on the above experiments that this guanine-rich DNA presents an ascribed equilibrium between G-quadruplex and unfolded structure in solution. A TBA molecule in solution can transform between the two forms. The equilibrium formation constant of G-quadruplex K_f can be defined as $K_f = \frac{[\mathrm{TBA_G}]}{[\mathrm{TBA_L}]}$, where $[\mathrm{TBA_G}]$ is the concentration of G-quadruplex (folded), $[\mathrm{TBA_L}]$ is the concentration of linear DNA (unfolded). Because $[\mathrm{TBA_L}]$ is proportional to the frequency of short event occurrence $f_{\mathrm{TBA_L}}$, $[\mathrm{TBA_L}]$ can be calculated using $f_{\mathrm{TBA_L}} = \alpha_{\mathrm{TBA_L}} \cdot [\mathrm{TBA_L}]$, where $\alpha_{\mathrm{TBA_L}}$ is the rate constant of linear-form DNA translocation. $\alpha_{\mathrm{TBA_L}}$ cannot be obtained from the mixed events of G-quadruplex and linear DNA. Instead, we can use the rate constant from control DNA of $\mathrm{Ctrl_2}$, $\alpha_{\mathrm{Ctrl_2}}$, as the linear-form DNA translocation rate for an approximate calculation. This is because unfolded TBA and $\mathrm{Ctrl_2}$ share the same sequence length, 73% of their nucleotides, and very similar translocation characteristics. For these reasons, it can be defined as $[\mathrm{TBA_L}] = \frac{f_{\mathrm{TBA_L}}}{f_{\mathrm{Ctrl_2}}}[\mathrm{Ctrl_2}]$. The G-quadruplex equilibrium formation constant is $K_f = \frac{[\mathrm{TBA_G}]}{[\mathrm{TBA_L}]} = \frac{[\mathrm{TBA}] - [\mathrm{TBA_L}]}{[\mathrm{TBA_L}]} = \frac{f_{\mathrm{Ctrl_2}} - f_{\mathrm{TBA_L}}}{f_{\mathrm{TBA_L}}}$ (where $[\mathrm{TBA}] = [\mathrm{Ctrl_2}]$). The calculated K_f for the TBA G-quadruplex has been found to be 7.0 in K^+, 4.6 in NH_4^+, 4.2 in Ba^{2+}, 2.8 in Cs^+, 2.3 in Na^+, and 1.5 in Li^+ (Fig. 4a). These equilibrium constants and their orders with the ion species are comparable to that found by other techniques [71,75], and are consistent with the conclusion that ions with a radius of 1.3–1.5 Å stabilize the G-quadruplex form at the most [71].

The unfolding rate constant for G-quadruplex can be expressed as $k_u = 1/\tau$, where τ is the lifetime of G-quadruplex in aqueous phase. We have experimentally verified that the unfolding of G-quadruplex in the nanocavity is a spontaneous process (voltage-independent), so the duration of long blocks is the lifetime of the G-quadruplex in the nanocavity. Our simulation also showed that the duration of long-lived events τ_G is identical

to the lifetime of the G-quadruplex in the solution phase (suppl. of [69]), i.e. $\tau = \tau_G$. Therefore $k_u = 1/\tau_G$. Using this expression, τ_G in different cations has been measured: ≈17 s in K^+, Ba^{2+}, and Li^+, 12 s in Cs^+, 4 s in NH_4^+ and 0.35 s in Na^+. Based on τ_G, k_u can be calculated to be 0.061 s^{-1} in Ba^{2+}, 0.066 s^{-1} in K^+, 0.065 s^{-1} in Li^+, 0.082 s^{-1} in Cs^+, 2.9 s^{-1} in Na^+, and 0.25 s^{-1} in NH_4^+ (Fig. 4b). With K_f and k_u, the folding rate constant K_f can be calculated using $K_f = \frac{K_f}{k_u}$. They are 6.5 s^{-1} in Na^+, 1.1 in NH_4^+, 0.46 s^{-1} in K^+, 0.25 s^{-1} in Ba^{2+}, 0.23 s^{-1} in Cs^+, and 0.095 s^{-1} in Li^+ (Fig. 4b).

2.7. Correlating G-quadruplex volume with its formability

It has been observed that the conductance of the G-quadruplex block varies with cation species. The relative amount of current blocked by the G-quadruplex was calculated to be $\frac{\Delta I}{I}$ (where I is the pore current and ΔI is the current reduction by G-quadruplex). The blocking percentage is an indicator of the volume of the G-quadruplex. Assuming all the G-quadruplexes are trapped in the same position in the nanocavity, larger G-quadruplex size causes greater blockage. Based on the block level, we can compare the relative volumes of the different G-quadruplexes formed using different cations. $\frac{\Delta I}{I}$ shows that Li^+ has the largest G-quadruplex, capable of blocking 50% of the current, and Ba^{2+} has the smallest complex, blocking 35%. The relative amount of current blocked has been found to be correlated with equilibrium formation constant of the G-quadruplex (Fig. 4a). In order to verify that the level of blockage is induced by the physical volume of the G-quadruplex, fixed-size molecule of beta-cyclodextrin (βCD) were introduced in the presence of Li^+ and Ba^{2+}. Unlike G-quadruplexes, the rigid ring molecule βCD does not bind metal ions, and its relative amount of blockage is cation-independent, 62.3% for Li^+ and 64% for Ba^{2+} (suppl. of [69]). This confirmed that the significant differences in current block percentage are associated with the volumes of G-quadruplexes of different cation species. This can be considered an advantage of the nanopore method because the volume of single molecules can be determined without crystallography or NMR.

2.8. Interaction between the G-quadruplex aptamer and ligand

TBA is a G-quadruplex aptamer. We selected it for this *in vitro* study using systematic evolution of ligands by exponential enrichment (SELEX) to determine that it would bind specifically with thrombin. Studying the interactions between aptamers and their protein ligands is important in both biosensor design and therapy [62]. However, most proteins, including thrombin, are larger than the nanopore. They cannot enter the pore to block the pore conductance. Recently, Bayley's group proposed a nanopore method for single-molecule observation of TBA:thrombin interactions [90] (Fig. 5a). This method involved a hetero-heptameric αHL pore in which only one of its seven subunits was chemically attached to an adapter oligonucleotide at the cysteine outside the pore opening. The adapter sequence is complementary with an oligonucleotide tag that is attached to TBA such that a single TBA molecule can be immobilized to the adapter through hybridization. When a single thrombin reversibly binds and is released from the immobilized TBA, the conformational change of the complex causes a slight but characteristic change in nanopore conductance (Fig. 5b). In this way, presence or absence of thrombin binding can be determined. The durations of the two states can be used to calculate the thrombin on-rate (k_{on} = 1.97 ± 0.01 × 10^7 M^{-1} s^{-1}) and off-rate (k_{off} = 1.5 ± 0.1 s^{-1}). Their ratio k_{off}/k_{on} should be the equilibrium constant K_d (77 ± 6 nM, in agreement with the range of 20–450 nM in early reports [64,91]). Because the adapter is a universal oligonucleotide, any aptamer with the same complementary tag can be immobilized. In this way, this system may be used to detect any protein as long as the binding of that protein can alter nanopore current.

3. Discussion of nanopore technology

In this report, we introduce nanopore technology as an effective approach to the investigation of single G-quadruplexes and their interactions with protein ligands. The G-quadruplex has also been studied using other single-molecule methods, including fluorescence resonance energy transfer (FRET) spectroscopy [82,84,85,92], and atomic force microscopy (AFM) [93-95]. Unlike these single molecule approaches, the nanopore electrical detection is a label-free method and does not need the attachment of probing agents such as fluorophores or immobilization on solid surfaces for observation. This facilitates the study of the G-quadruplex in its native state without any chemical modifications. This method's low noise signal makes it much easier to identify single molecule using the nanopore method than using methods such as fluorescence, which requires the removal of the background signal. Because the nanopore conductance is stable (due to the stable pore structure), results are highly reproducible. Among these single-molecule methods, the nanopore experiment is relatively simple and easy to operate and the instruments required are low-cost. However, one limitation of the nanopore detection is that it requires detection in salt solutions with concentrations over 100 mM. Low salt concentration or salt-free conditions reduce the nanopore conductance, weakening discriminatory ability. Small pore size is another issue. Folded RNA and DNA, including various quadruplexes similar or smaller than the pore in size (2.6 nm at the entrance), can be investigated using the nanopore method, but larger molecules than the pore size must be detected by use of a tag method similar to that described in Fig. 5 [68]. Once the molecule is attaching to a tag such as an oligonucleotide extension at the end of the strand, which does not involve in the folded structure, the tag can interact with the nanopore. This makes it possible to investigate the stability of folded structures by measuring interaction time and electrical force in various cation solutions.

In the nanopore method, the single-molecule signatures (characteristic nanopore blockages) are the key to distinguishing the pore's different molecular configurations. Through analysis of these signatures, we can identify nucleic acid fragments in the folded and unfolded forms, observe the manner in which cations regulate the folding/unfolding reactions of the G-quadruplex, and assess interactions between the G-quadruplex and proteins. The results of the nanopore observations are generally consistent with those of previous studies. The cation species-dependent G-quadruplex stability ($K^+ > NH_4^+ \sim Ba^{2+} > Cs^+ \sim Na^+ > Li^+$) and the equilibrium properties of TBA:thrombin complex are consistent across studies. However, the nanopore method also provides information on issues that have only rarely been studied. For example, although the equilibrium properties of G-quadruplex in Na^+ and Li^+ are similar, their kinetic properties are dramatically different: the Na^+-quadruplex folds and unfolds most rapidly, and the Li^+-quadruplex folds and unfolds most slowly. Also, the volumes of TBA G-quadruplexes change slightly with different cations. Although we have demonstrated that the nanopore method can be used to investigate single G-quadruplex reaction kinetics, this method needs further development, especially with an eye toward combining it with other methods. This may be very valuable to the study of the mechanism governing these molecular processes. Toward this goal, we here suggest a series of high-impact experiments: First, tracking the G-quadruplex kinetic pathway, which varies with temperature and pH, would improve our understanding of its thermodynamic properties. Analysis of the properties of G-quadruplex in the presence of multiple cation species at different concentrations would allow investigation of ion exchange within G-quadruplexes (in preparation). Investigation of single-guanine substitutions would allow us to determine the role of individual guanines in the stability of the G-quadruplex. The nanopore method can also be used as a molecular force microscope. The voltage across the nanopore can pull the designed tag attached to the G-quadruplex, thus highlighting the unfolding of the G-

quadruplex and dissociation of G-quadruplex-protein complex within the nanopore. This would allow researchers to measure the bond strength affecting these interactions.

Acknowledgments

This investigation was supported by NSF 0546165 and NIH1R01GM079613. This investigation was conducted in a facility constructed with support from the Research Facilities Improvement Program Grant C06-RR-016489-01 from the National Center for Research Resources, National Institutes of Health.

References

1. Bayley H. Bioorg Chem. 1995; 23:340–354.
2. Walker B, Braha O, Cheley S, Bayley H. Chem Biol. 1995; 2:99–105. [PubMed: 9383410]
3. Braha O, Walker B, Cheley S, Kasianowicz JJ, Song LZ, Gouaux JE, Bayley H. Chem Biol. 1997; 4:497–505. [PubMed: 9263637]
4. Song LZ, Hobaugh MR, Shustak C, Cheley S, Bayley H, Gouaux JE. Science. 1996; 274:1859–1866. [PubMed: 8943190]
5. Bayley H, Cremer PS. Nature. 2001; 413:226–230. [PubMed: 11557992]
6. Branton D, Deamer DW, Marziali A, Bayley H, Benner SA, Butler T, Di Ventra M, Garaj S, Hibbs A, Huang XH, Jovanovich SB, Krstic PS, Lindsay S, Ling XSS, Mastrangelo CH, Meller A, Oliver JS, Pershin YV, Ramsey JM, Riehn R, Soni GV, Tabard-Cossa V, Wanunu M, Wiggin M, Schloss JA. Nat Biotechnol. 2008; 26:1146–1153. [PubMed: 18846088]
7. Gu LQ, Shim JW. Analyst. 2010; 135:441–451. [PubMed: 20174694]
8. Deamer D. Annu Rev Biophys. 2010; 39:79–90. [PubMed: 20192777]
9. Bayley H, Jayasinghe L. Mol Membr Biol. 2004; 21:209–220. [PubMed: 15371010]
10. Howorka S, Siwy Z. Chem Soc Rev. 2009; 38:2360–2384. [PubMed: 19623355]
11. Ma L, Cockroft SL. ChemBioChem. 2010; 11:25–34. [PubMed: 19938028]
12. Majd S, Yusko EC, Billeh YN, Macrae MX, Yang J, Mayer M. Curr Opin Biotechnol. 2010; 21:439–476. [PubMed: 20561776]
13. Movileanu L. Trends Biotechnol. 2009; 27:333–341. [PubMed: 19394097]
14. Olasagasti F, Lieberman KR, Benner S, Cherf GM, Dahl JM, Deamer DW, Akeson M. Nat Nanotechnol. 2010; 5:798–806. [PubMed: 20871614]
15. Liu AH, Zhao QT, Guan XY. Anal Chim Acta. 2010; 675:106–115. [PubMed: 20800721]
16. Clarke J, Wu HC, Jayasinghe L, Patel A, Reid S, Bayley H. Nat Nanotechnol. 2009; 4:265–270. [PubMed: 19350039]
17. Soni GV, Meller A. Clin Chem. 2007; 53:1996–2001. [PubMed: 17890440]
18. Bayley H. Curr Opin Chem Biol. 2006; 10:628–637. [PubMed: 17113816]
19. McNally B, Singer A, Yu ZL, Sun YJ, Weng ZP, Meller A. Nano Lett. 2010; 10:2237–2244. [PubMed: 20459065]
20. Derrington IM, Butler TZ, Collins MD, Manrao E, Pavlenok M, Niederweis M, Gundlach JH. Proc Natl Acad Sci USA. 2010; 107:16060–16065. [PubMed: 20798343]
21. Gu LQ, Braha O, Conlan S, Cheley S, Bayley H. Nature. 1999; 398:686–690. [PubMed: 10227291]
22. Movileanu L, Howorka S, Braha O, Bayley H. Nat Biotechnol. 2000; 18:1091–1095. [PubMed: 11017049]
23. Kasianowicz JJ, Brandin E, Branton D, Deamer DW. Proc Natl Acad Sci USA. 1996; 93:13770–13773. [PubMed: 8943010]
24. Vercoutere W, Winters-Hilt S, Olsen H, Deamer D, Haussler D, Akeson M. Nat Biotechnol. 2001; 19:248–252. [PubMed: 11231558]
25. Howorka S, Cheley S, Bayley H. Nat Biotechnol. 2001; 19:636–639. [PubMed: 11433274]
26. Mathe J, Visram H, Viasnoff V, Rabin Y, Meller A. Biophys J. 2004; 87:3205–3212. [PubMed: 15347593]

27. Nakane J, Wiggin M, Marziali A. Biophys J. 2004; 87:615–621. [PubMed: 15240494]
28. Ashkenasy N, Sanchez-Quesada J, Bayley H, Ghadiri MR. Angew Chem Int Ed. 2005; 44:1401–1404.
29. Astier Y, Braha O, Bayley H. J Am Chem Soc. 2006; 128:1705–1710. [PubMed: 16448145]
30. Jung Y, Cheley S, Braha O, Bayley H. Biochemistry – US. 2005; 44:8919–8929.
31. Braha O, Gu LQ, Zhou L, Lu XF, Cheley S, Bayley H. Nat Biotechnol. 2000; 18:1005–1007. [PubMed: 10973225]
32. Cheley S, Gu LQ, Bayley H. Chem Biol. 2002; 9:829–838. [PubMed: 12144927]
33. Wang Y, Zheng DL, Tan QL, Wang MX, Gu LQ. Nat Nanotechnol. 2011; 6:668–674. [PubMed: 21892163]
34. Gu LQ, Dalla Serra M, Vincent JB, Vigh G, Cheley S, Braha O, Bayley H. Proc Natl Acad Sci USA. 2000; 97:3959–3964. [PubMed: 10760267]
35. Gu LQ, Cheley S, Bayley H. Proc Natl Acad Sci USA. 2003; 100:15498–15503. [PubMed: 14676320]
36. Hornblower B, Coombs A, Whitaker RD, Kolomeisky A, Picone SJ, Meller A, Akeson M. Nat Methods. 2007; 4:315–317. [PubMed: 17339846]
37. Sauer-Budge AF, Nyamwanda JA, Lubensky DK, Branton D. Phys Rev Lett. 2003; 90:23801-1–23801-4.
38. Kang XF, Cheley S, Rice-Ficht AC, Bayley H. J Am Chem Soc. 2007; 129:4701–4705. [PubMed: 17375923]
39. Shim JW, Gu LQ. Anal Chem. 2007; 79:2207–2213. [PubMed: 17288404]
40. Henderson E, Hardin CC, Walk SK, Tinoco I, Blackburn EH. Cell. 1987; 51:899–908. [PubMed: 3690664]
41. Sen D, Gilbert W. Nature. 1988; 334:364–366. [PubMed: 3393228]
42. Macaya RF, Schultze P, Smith FW, Roe JA, Feigon J. Proc Natl Acad Sci USA. 1993; 90:3745–3749. [PubMed: 8475124]
43. Burge S, Parkinson GN, Hazel P, Todd AK, Neidle S. Nucleic Acids Res. 2006; 34:5402–5415. [PubMed: 17012276]
44. Qin Y, Hurley LH. Biochimie. 2008; 90:1149–1171. [PubMed: 18355457]
45. Brooks TA, Kendrick S, Hurley L. FEBS J. 2010; 277:3459–3469. [PubMed: 20670278]
46. Huppert JL. FEBS J. 2010; 277:3452–3458. [PubMed: 20670279]
47. Sharma S, Doherty KM, Brosh RM Jr. Curr Med Chem Anticancer Agents. 2005; 5:183–199. [PubMed: 15992349]
48. Neidle S. Curr Opin Struct Biol. 2009; 19:239–250. [PubMed: 19487118]
49. Neidle S, Read MA. Biopolymers. 2000; 56:195–208. [PubMed: 11745111]
50. Davis JT. Angew Chem Int Ed. 2004; 43:668–698.
51. Parkinson GN, Lee MPH, Neidle S. Nature. 2002; 417:876–880. [PubMed: 12050675]
52. Phan AT, Kuryavyi V, Ma JB, Faure A, Andreola ML, Patel DJ. Proc Natl Acad Sci USA. 2005; 102:634–639. [PubMed: 15637158]
53. Todd AK, Johnston M, Neidle S. Nucleic Acids Res. 2005; 33:2901–2907. [PubMed: 15914666]
54. Rankin S, Reszka AP, Huppert J, Zloh M, Parkinson GN, Todd AK, Ladame S, Balasubramanian S, Neidle S. J Am Chem Soc. 2005; 127:10584–10589. [PubMed: 16045346]
55. Wang Y, Patel DJ. Structure. 1994; 2:1141–1156. [PubMed: 7704525]
56. Wang Y, Patel DJ. J Mol Biol. 1995; 251:76–94. [PubMed: 7643391]
57. Fletcher TM, Sun DK, Salazar M, Hurley LH. Biochemistry – US. 1998; 37:5536–5541.
58. Dexheimer TS, Sun D, Hurley LH. J Am Chem Soc. 2006; 128:5404–5415. [PubMed: 16620112]
59. Siddiqui-Jain A, Grand CL, Bearss DJ, Hurley LH. Proc Natl Acad Sci USA. 2002; 99:11593–11598. [PubMed: 12195017]
60. Phan AT, Kuryavyi V, Burge S, Neidle S, Patel DJ. J Am Chem Soc. 2007; 129:4386–4392. [PubMed: 17362008]
61. Heyduk T, Heyduk E. Nat Biotechnol. 2002; 20:171–176. [PubMed: 11821863]

62. Bock LC, Griffin LC, Latham JA, Vermaas EH, Toole JJ. Nature. 1992; 355:564–566. [PubMed: 1741036]
63. Ho HA, Leclerc M. J Am Chem Soc. 2004; 126:1384–1387. [PubMed: 14759196]
64. Huang CC, Cao ZH, Chang HT, Tan WH. Anal Chem. 2004; 76:6973–6981. [PubMed: 15571349]
65. Alberti P, Mergny JL. Proc Natl Acad Sci USA. 2003; 100:1569–1573. [PubMed: 12574521]
66. Li JWJ, Tan WH. Nano Lett. 2002; 2:315–318.
67. Davis JT, Spada GP. Chem Soc Rev. 2007; 36:296–313. [PubMed: 17264931]
68. Shim JW, Gu LQ. J Phys Chem B. 2008; 112:8354–8360. [PubMed: 18563930]
69. Shim JW, Tan QL, Gu LQ. Nucleic Acids Res. 2009; 37:972–982. [PubMed: 19112078]
70. Wang KY, Krawczyk SH, Bischofberger N, Swaminathan S, Bolton PH. Biochemistry – US. 1993; 32:11285–11292.
71. Kankia BI, Marky LA. J Am Chem Soc. 2001; 123:10799–10804. [PubMed: 11686680]
72. Padmanabhan K, Padmanabhan KP, Ferrara JD, Sadler JE, Tulinsky A. J Biol Chem. 1993; 268:17651–17654. [PubMed: 8102368]
73. Marathias VM, Bolton PH. Nucleic Acids Res. 2000; 28:1969–1977. [PubMed: 10756199]
74. Mao XA, Marky LA, Gmeiner WH. J Biomol Struct Dyn. 2004; 22:25–33. [PubMed: 15214802]
75. Hardin CC, Perry AG, White K. Biopolymers. 2000; 56:147–194. [PubMed: 11745110]
76. Jing NJ, Hogan ME. J Biol Chem. 1998; 273:34992–34999. [PubMed: 9857031]
77. Olsen CM, Gmeiner WH, Marky LA. J Phys Chem B. 2006; 110:6962–6969. [PubMed: 16571009]
78. Smirnov I, Shafer RH. Biochemistry – US. 2000; 39:1462–1468.
79. Zhao Y, Kan ZY, Zeng ZX, Hao YH, Chen H, Tan Z. J Am Chem Soc. 2004; 126:13255–13264. [PubMed: 15479079]
80. Simonsson T, Sjoback R. J Biol Chem. 1999; 274:17379–17383. [PubMed: 10358100]
81. Green JJ, Ladame S, Ying LM, Klenerman D, Balasubramanian S. J Am Chem Soc. 2006; 128:9809–9812. [PubMed: 16866537]
82. Ying LM, Green JJ, Li HT, Klenerman D, Balasubramanian S. Proc Natl Acad Sci USA. 2003; 100:14629–14634. [PubMed: 14645716]
83. Okumus B, Ha T. Methods Mol Biol. 2010; 608:81–96. [PubMed: 20012417]
84. Jena PV, Shirude PS, Okumus B, Laxmi-Reddy K, Godde F, Huc I, Balasubramanian S, Ha T. J Am Chem Soc. 2009; 131:12522–12523. [PubMed: 19685880]
85. Shirude PS, Okumus B, Ying LM, Ha T, Balasubramanian S. J Am Chem Soc. 2007; 129:7484–7485. [PubMed: 17523641]
86. Bhakdi S, Tranumjensen J. Microbiol Rev. 1991; 55:733–751. [PubMed: 1779933]
87. Montal M, Mueller P. Proc Natl Acad Sci USA. 1972; 69:3561–3566. [PubMed: 4509315]
88. Jing NJ, Rando RF, Pommier Y, Hogan ME. Biochemistry – US. 1997; 36:12498–12505.
89. Fialova M, Kypr J, Vorlickova M. Biochem Biophys Res Commun. 2006; 344:50–54. [PubMed: 16616893]
90. Rotem D, Jayasinghe L, Salichou M, Bayley H. J Am Chem Soc. 2012; 134:2781–2787. [PubMed: 22229655]
91. German I, Buchanan DD, Kennedy RT. Anal Chem. 1998; 70:4540–4545. [PubMed: 9823713]
92. Ishitsuka Y, Okumus B, Arslan S, Chen KH, Ha T. Anal Chem. 2010; 82:9694–9701. [PubMed: 21038883]
93. Kan ZY, Lin Y, Wang F, Zhuang XY, Zhao Y, Pang DW, Hao YH, Tan Z. Nucleic Acids Res. 2007; 35:3646–3653. [PubMed: 17488850]
94. Sannohe Y, Endo M, Katsuda Y, Hidaka K, Sugiyama H. J Am Chem Soc. 2010; 132:16311–16313. [PubMed: 21028867]
95. Wang H, Nora GJ, Ghodke H, Opresko PL. J Biol Chem. 2011; 286:7479–7489. [PubMed: 21183684]
96. Schultze P, Macaya RF, Feigon J. J Mol Biol. 1994; 235:1532–1547. [PubMed: 8107090]
97. Drew HR, Wing RM, Takano T, Broka C, Tanaka S, Itakura K, Dickerson RE. Proc Natl Acad Sci -Biol. 1981; 78:2179–2183.

98. Padmanabhan K, Tulinsky A. Acta Crystallogr D. 1996; 52:272–282. [PubMed: 15299700]

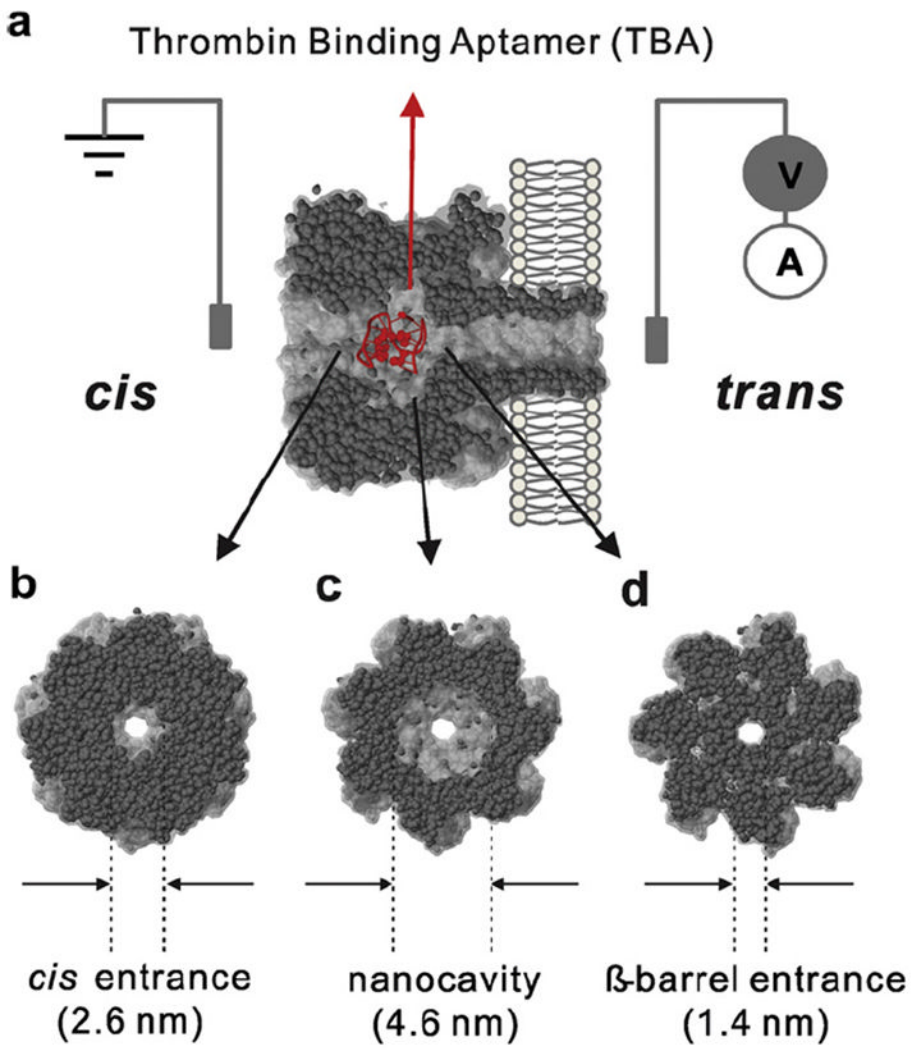

Fig. 1.

Structure of the αHL protein pore and schematic diagram of recording configuration. Images of molecular structures were constructed using Jmol, an open-source Java viewer for chemical structures in 3D (http://www.jmol.org/). (a) Cross-sectional view of αHL (PDB ID: 7AHL [4]) inserted into planar lipid bilayer. Mushroom-shape cap faces to *cis* solution which is connected to ground and β-barrel faces *trans* at voltage command. TBA (PDB ID: 148D [96]) G-quadruplex is located in the nanocavity. (b–d) Diameters of (b) *cis* entrance (2.6 nm), (c) nanocavity (4.6 nm), and (d) constriction site of β-barrel (1.4 nm). All molecular structures in (b–d) are top–down cross-sectional views.

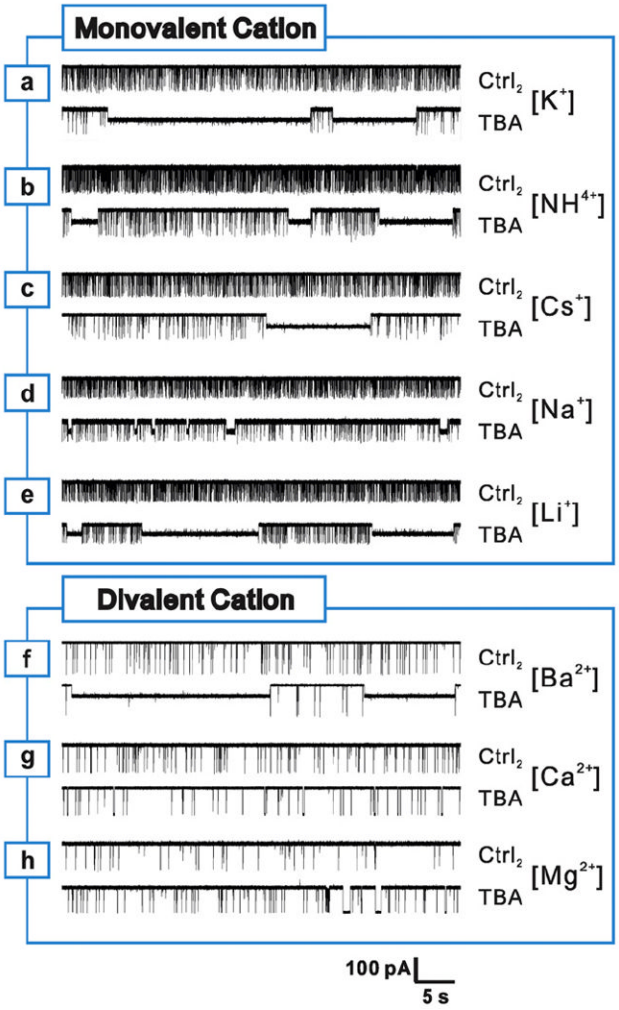

Fig. 2.

Representative current traces for TBA and $Ctrl_2$ (control) in various salt solutions. In each panel, the upper trace shows $Ctrl_2$ and the lower one shows TBA. (a) K^+; (b) NH_4^+; (c) Cs^+; (d) Na^+; (e) Li^+; (f) Ba^{2+}; (g) Ca^{2+}; and (h) Mg^{2+}. All traces were recorded at +100 mV. Traces were extracted from original recordings and not adopted from published works.

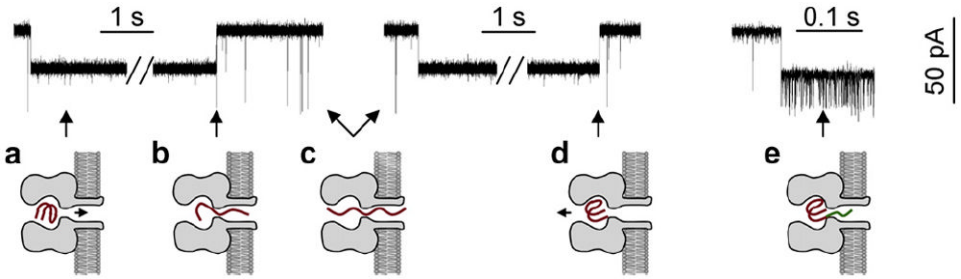

Fig. 3.

(a–d) Representative current block signature events and models for TBA and tagged-TBA (e) interacting with nanopores. (a) The long partial block shows the G-quadruplex (folded TBA) trapped in nanocavity. (b) G-quadruplex finally unfolds spontaneously in the nanocavity and leaves the nanopore, producing a fast-deep terminal-spike. (c) The unfolded TBA in linear form in the solution translocates through the nanopore, generating a short-deep current block. (d) The trapped G-quadruplex in the nanocavity can also escape the pore to the *cis* side without unfolding, not producing terminal-spike as indicated. (e) The overhang of the tagged-TBA enters the b-barrel when trapped in the pore, generating reversible level-2 block upon the long block. Traces were extracted from original recordings and not adopted from published works.

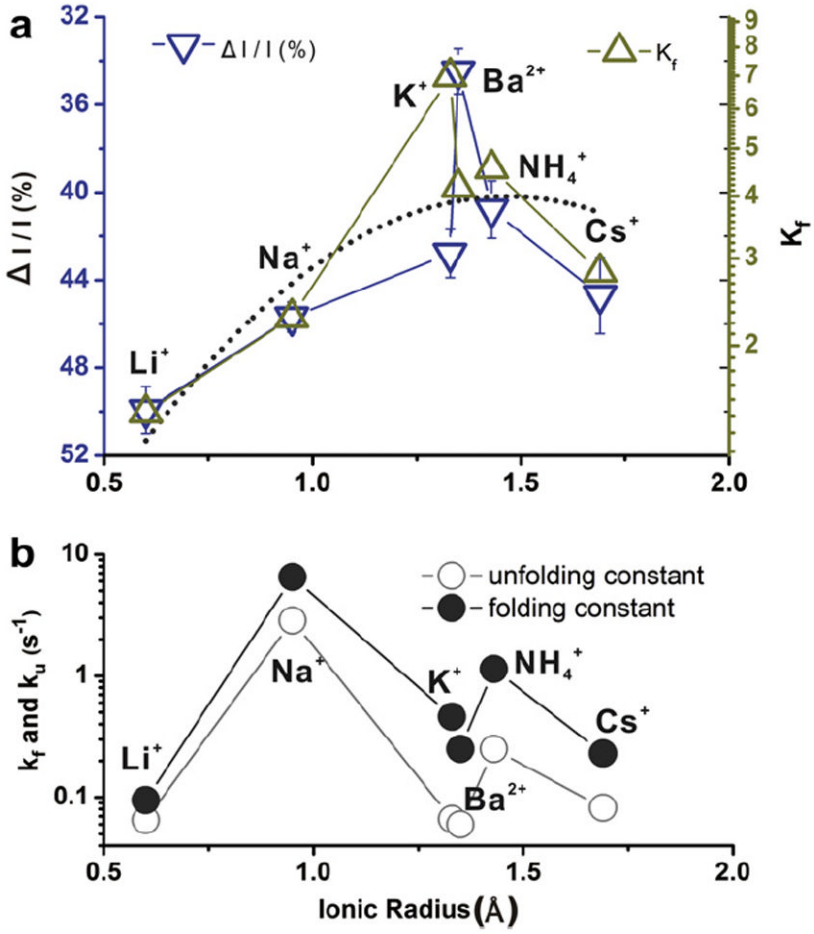

Fig. 4.

Equilibrium and kinetic constants for G-quadruplex in various cations. (a) Equilibrium formation constant of G-quadruplex (K_f) and its correlation with current blocking percentage ($\Delta I/I$) of G-quadruplex. (b) Folding (K_f) and unfolding (k_u) constants for TBA G-quadruplex. Data were adopted from a previous study [79].

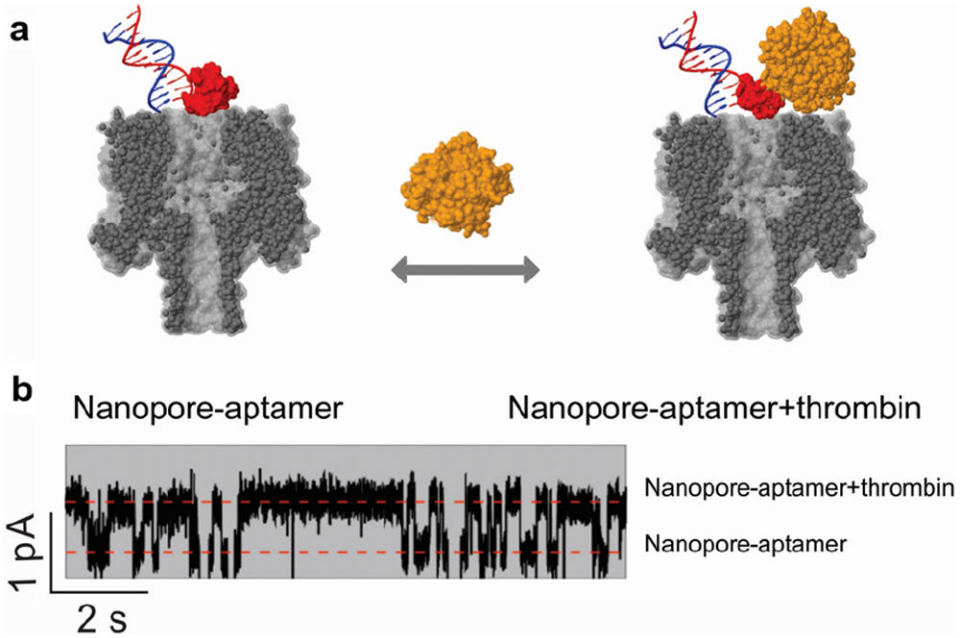

Fig. 5.

Investigation of TBA: Thrombin interactions within a protein nanopore. (a) Model showing molecular structure of the nanopore-TBA system for detection of thrombin. The adapter oligonucleotide was cross-linked with the cysteine of one subunit at the pore's *cis* opening. The tagged-TBA used the tag to hybridize with the adapter for immobilization. Aptamers (right) containing thrombin and (left) lacking thrombin all bound block the pore to different extents. (b) Representative current trace showing two transitions between two current levels that correspond to the states without (upper) and with (lower) thrombin bound. Images of molecular structures were constructed using Jmol, an open-source Java viewer for chemical structures in 3D (http://www.jmol.org/). dsDNA and TBA (PDB ID: 1BNA [97] and 148D [96]). Thrombin with TBA (PDB ID: 1HAP [98]).